

Supplementary Material

Main document: *A compositional model to assess expression changes from single-cell RNA-seq data*

Authors: Ma, Korthauer, Kendzierski, and Newton

Version: May 23, 2019

This supplement is organized to match the sectioning of the main document. In summary,

1. Introduction
 - R package
2. Modeling
 - Data Structure, Sampling Model, and Parameters
 - Proof of Theorem 2
 - Method Structure and Clustering
 - EBSeq
 - modalClust
 - Randomized K –means
 - Selecting K
 - Double Dirichlet Mixture
 - Proof of Properties 1-6 and Theorem 3
3. Numerical Experiments
 - Synthetic data, splatter
 - Empirical study, conquer and Null case
 - Robustness
4. Posterior consistency
 - proof of theorem 4

1. Introduction.

1.1. *R package.* We developed a R package `scDDboost` providing clustering, EBSeq and final PDD calculation. Details can be found at github site <https://github.com/wiscstatman/scDDboost>

2. Modeling.

2.1. Data Structure, Sampling Model, and Parameters.

PROOF OF THEOREM 2. Recall $\theta = (\phi, \psi, \mu, \sigma)$. Through the sampling procedure of our model (Figure 3), assuming a known number of cells within each condition (n_1, n_2) . We have z^1, z^2 are multinomial draw given ϕ and ψ , thus the generation of y, z only depends on (ϕ, ψ) . Also given z , $X_{g,c}$ is sampled through $NB(\mu_{g,z_c}, \sigma_g)$, and only depends on (μ, σ) . Thus $P(X, y, z | \theta) = P(y, z | \phi, \psi) P(X | z, \mu, \sigma)$, and we independently give priors for (μ, σ) and (ϕ, ψ) . By the Baye's rule,

$$\begin{aligned} P(\theta | X, y, z) &\propto P(X, y, z | \theta) P(\theta) \\ P(X, y, z | \theta) P(\theta) &= P(y, z | \phi, \psi) P(X | z, \mu, \sigma) P(\mu, \sigma | z) P(\phi, \psi) \\ P(\phi, \psi | y, z) &\propto P(y, z | \phi, \psi) P(\phi, \psi) \\ P(\mu, \sigma | X, z) &\propto P(X | z, \mu, \sigma) P(\mu, \sigma | z) \\ \text{Thus } P(\theta | X, y, z) &\propto P(\phi, \psi | y, z) P(\mu, \sigma | X, z) \end{aligned}$$

From above we know

1. Given condition and subtypes label y, z , $(\phi, \psi) \perp X$
2. Given X and z , $(\mu, \sigma) \perp y$
3. Given X, y and z , $(\phi, \psi) \perp (\mu, \sigma)$

Thus we have $P(A_\pi \cap M_{g,\pi} | X, y, z) = P(A_\pi | y, z) P(M_{g,\pi} | X, z)$. □

2.2. Method Structure and Clustering.

2.2.1. *EBSeq.* In this subsection, we go through how we implemented and modified EBSeq to get $P(M_{g,\pi} | X, z)$.

Suppose we have K subtypes, let $X_g^I = X_{g,1}^I, \dots, X_{g,S_1}^I$ denote transcripts at gene g from subtype $I, I = 1, \dots, K$. The EBSeq model assumes that counts within subtype I are distributed as Negative Binomial: $X_{g,s}^I | r_{g,s}, q_g^I \sim NB(r_{g,s}, q_g^I)$. Due to sample-specific size factor in the raw counts, r is made sample-specific. However, we are dealing with normalized counts rather than raw counts in EBSeq, we instead make r shared at gene level across all samples, i.e. $X_{g,s}^I | \sigma_g, q_g^I \sim NB(\sigma_g, q_g^I)$

$$P(X_{g,s}^I | \sigma_g, q_g^I) = \binom{X_{g,s}^I + \sigma_g - 1}{X_{g,s}^I} (1 - q_g^I)^{X_{g,s}^I} (q_g^I)^{\sigma_g}$$

and $\mu_{g,s}^I = \sigma_g(1 - q_g^I)/q_g^I$; For ease in later deriving the density kernel f , we use q rather than μ to parameterize the NB.

Following EBSeq, we assume a prior distribution on $q_g^I : q_g^I | \alpha, \beta^g \sim \text{Beta}(\alpha, \beta^g)$. The hyperparameter α is shared by the whole genome and β^g is gene-specific.

We force the size factor to be 1 for all cells and use the same procedure as EBSeq to estimate the failure parameter σ_g . Namely, we have

1. gene-level sample mean $m_g = \frac{1}{n} \sum_{s=1}^n X_{g,s}$, where $n = n_1 + n_2$ is the total number of cells
2. average of sample variances over subtypes $v_g = \frac{1}{K} \sum_{l=1}^K v_g^I$.
3. v_g^I is the unadjusted sample variance for subtype I , i.e. $v_g^I = \frac{1}{n^I} \sum_{s, z_s=I} (X_{g,s} - m_g^I)^2$ where m_g^I is the sample mean within subtype I and n^I is the number of cells within subtype I .

We estimate the pooled over-dispersion rate by $o_g = \frac{v_g}{m_g}$ and obtain $\sigma_g = m_g \frac{o_g}{1-o_g}$ from the first moment of NB.

Our target is to quantify the expression pattern between K groups,

$$M_{g,\pi} = \{\theta \in \Theta : \mu_{g,k} = \mu_{g,k'} \iff k, k' \in b, b \in \pi\}.$$

For example, if $K = 3$, there are 5 expression patterns: P_1, P_2, \dots, P_5 . Comparison between μ is equivalent to comparison between q .

$$\begin{aligned} P1 : q_g^1 &= q_g^2 = q_g^3 \\ P2 : q_g^1 &= q_g^2 \neq q_g^3 \\ P3 : q_g^1 &\neq q_g^2 = q_g^3 \\ P4 : q_g^1 &= q_g^3 \neq q_g^2 \\ P5 : q_g^1 &\neq q_g^2 \neq q_g^3 \text{ and } q_g^1 \neq q_g^3 \end{aligned}$$

Under the assumption that two groups I and J share the same q_g we can pool the counts from the two groups by viewing them as sampled from same distribution, i.e. $X_g^{I,J} | \sigma_g, q_g \sim \text{NB}(\sigma_g, q_g)$, $q_g | \alpha, \beta^g \sim \text{Beta}(\alpha, \beta^g)$. Then we obtain the prior predictive function $f(X_g^{I,J}) = \int_0^1 P(X_g^{I,J} | r_g, q_g) * P(q_g | \alpha, \beta^g) dq_g = \left[\prod_{s=1}^S \binom{X_{g,s} + \sigma_g - 1}{X_{g,s}} \right] \frac{\text{Beta}(\alpha + \sum_{s=1}^S \sigma_g, \beta^g + \sum_{s=1}^S X_{g,s})}{\text{Beta}(\alpha, \beta^g)}$. Consequently, the prior predictive function for $P1, \dots, P5$ is

$$\begin{aligned}
h_1^g(X_g) &= f(X_g^{1,2,3}) \\
h_2^g(X_g) &= f(X_g^{1,2})f(X_g^3) \\
h_3^g(X_g) &= f(X_g^1)f(X_g^{2,3}) \\
h_4^g(X_g) &= f(X_g^{1,3})f(X_g^2) \\
h_5^g(X_g) &= f(X_g^1)f(X_g^2)f(X_g^3)
\end{aligned}$$

where $h_i^g(X_g) = P(X_g|M_{g,\pi_i},z)$ for associated π_i . Then the marginal distribution of counts X_g is $\sum_{k=1}^5 p_k h_k^g(X_g)$, where the marginal $p_k = P(M_{g,\pi}|z)$ (shared by all genome). Thus, the posterior probability of an expression pattern k is obtained by:

$$\frac{p_k h_k(X_g)}{\sum_{k=1}^5 p_k h_k^g(X_g)}$$

In the optimization steps for determining the hyperparameters (α, β^g, p) , the computation and memory increase exponentially with the number of subtypes K . We use one-step EM as an approximation for the solution, α and β^g are updated through gradient ascent while p is updated by the explicit form of the maximizer of the log likelihood.

2.2.2. modalClust. In this section, we review the procedure of modal-clustering and proof the compatibility of density kernel from Poisson-Gamma model.

Product Partition Model

Let $X = (X_1, X_2, \dots, X_n)$ be a vector of observed data. Given a partition for the data $\pi = \{S_1, \dots, S_q\}$, where S_i are disjoint subsets of $\{1, 2, \dots, n\}$ and $\bigcup_{i=1}^q S_i = \{1, 2, \dots, n\}$, the likelihood for X satisfying such partition is

$$p(X|\pi) = \prod_{i=1}^q f(X_{S_i})$$

where X_{S_i} is the vector of observations corresponding to the items of component S_i . The component likelihood $f(X_S)$ is defined for any non-empty component S and can take any form. The partition π is the only parameter we are interested in. Any other parameters that may have been involved in the model have been integrated over their prior.

The prior distribution for a partition π is also taken as a product form. We use the MAP partition (maximizing the posterior $p(\pi|X) \propto p(X|\pi)p(\pi)$) as the estimated clustering.

[Dahl \(2009\)](#) demonstrated that by some choice of f and prior of π , we can reduce the time complexity of finding the MAP partition from factorial(n) to $O(n^2)$. The crucial

condition for f is the **non-overlapping** condition: if X_{S_1} and X_{S_2} are overlapped in the sense that $\min\{X_{S_2}\} < \max\{X_{S_1}\} < \max\{X_{S_2}\}$ or $\min\{X_{S_1}\} < \max\{X_{S_2}\} < \max\{X_{S_1}\}$, let $X_{S_1}^*$ and $X_{S_2}^*$ be the sets of swapping one pair of those overlapped terms and keep the other unchanged. Then $f(X_{S_1})f(X_{S_2}) \leq f(X_{S_1}^*)f(X_{S_2}^*)$.

Under the **non-overlapping** condition of density kernel f , we know that in order to be MAP, a partition π must satisfy that for any two blocks $b_1, b_2 \in \pi$, either $\max_{i \in b_1}(X_i) \leq \min_{j \in b_2}(X_j)$ or $\min_{i \in b_1}(X_i) \geq \max_{j \in b_2}(X_j)$. Thus we reduce the solution space and reduce the time complexity.

In the Poisson-Gamma Model we assume:

$$\begin{aligned} X_i | \pi, \lambda &\sim \text{Poisson}(X_i | \lambda_1 \mathbf{I}\{i \in S_1\} + \dots + \lambda_q \mathbf{I}\{i \in S_q\}) \\ \pi &\sim p(\pi) \\ \lambda_j &\sim \text{Gamma}(\alpha_0, \beta_0) \end{aligned}$$

where $p(\pi) \propto \prod_{i=1}^q \eta_0 \Gamma(|S_i|)$. Integrate out λ , $f(X_S)$ is obtained as:

$$f(X_S) = \frac{\beta^\alpha}{(|S| + \beta)^{\sum_{i \in S} X_i + \alpha}} \frac{\Gamma(\sum_{i \in S} X_i + \alpha)}{\Gamma(\alpha)} \frac{1}{\prod_{i \in S} X_i}$$

To apply modal-clustering on Poisson-Gamma model, we need to show the kernel $f(X_S)$ satisfies the **non-overlapping** condition.

PROOF. if X_{S_1} and X_{S_2} are overlapping, without loss of generality, we assume $\min\{X_{S_2}\} < \max\{X_{S_1}\} < \max\{X_{S_2}\}$, and we swap $\max\{X_{S_1}\}$ with $\min\{X_{S_2}\}$ and keep the rest unchanged or we could also swap $\max\{X_{S_1}\}$ with $\max\{X_{S_2}\}$. We denote the new set forming by swap of $\max\{X_{S_1}\}$ with $\min\{X_{S_2}\}$ as S_1^* and S_2^* and swap of $\max\{X_{S_1}\}$ with $\max\{X_{S_2}\}$ as S_1^{**}, S_2^{**} accordingly.

Then we need to show at least one of the following happens

- (1) $f(X_{S_1^*})f(X_{S_2^*}) \geq f(X_{S_1})f(X_{S_2})$
- (2) $f(X_{S_1^{**}})f(X_{S_2^{**}}) \geq f(X_{S_1})f(X_{S_2})$

Let $a = \max\{X_{S_1}\}$, $b = \min\{X_{S_2}\}$ and $c = \max\{X_{S_2}\}$. $h_1 = \sum_{i \in S_1} X_i - a$ and $h_2 =$

$\sum_{i \in S_2} X_i - b$, n_1 and n_2 are the number of elements in S_1 and S_2 . Then

$$\begin{aligned}
f(X_{S_1^*})f(X_{S_2^*}) &\geq f(X_{S_1})f(X_{S_2}) \\
&\iff \\
\frac{\Gamma(h_1 + a + \alpha)}{(n_1 + \beta)^{h_1 + a + \alpha}} \frac{\Gamma(h_2 + b + \alpha)}{(n_2 + \beta)^{h_2 + b + \alpha}} &\leq \frac{\Gamma(h_2 + a + \alpha)}{(n_2 + \beta)^{h_2 + a + \alpha}} \frac{\Gamma(h_1 + b + \alpha)}{(n_2 + \beta)^{h_1 + b + \alpha}} \\
&\iff \\
\frac{\Gamma(h_1 + a + \alpha)}{\Gamma(h_1 + b + \alpha)} \frac{\Gamma(h_2 + b + \alpha)}{\Gamma(h_2 + a + \alpha)} &\leq \left(\frac{n_1 + \beta}{n_2 + \beta}\right)^{a-b}
\end{aligned}$$

The left hand side of the above formula is $\text{LHS}_1 = \frac{(h_1 + b + \alpha) \dots (h_1 + a - 1 + \alpha)}{(h_2 + b + \alpha) \dots (h_2 + a - 1 + \alpha)}$ by the property of Gamma function and X_i are integers.

Similarly,

$$\begin{aligned}
f(X_{S_1^{**}})f(X_{S_2^{**}}) &\geq f(X_{S_1})f(X_{S_2}) \\
&\iff \\
\frac{\Gamma(h_2 + c + \alpha)}{\Gamma(h_2 + a + \alpha)} \frac{\Gamma(h_1 + a + \alpha)}{\Gamma(h_1 + c + \alpha)} &\leq \left(\frac{n_2 + \beta}{n_1 + \beta}\right)^{c-a}
\end{aligned}$$

The left hand side of above formula is $\text{LHS}_2 = \frac{(h_2 + a + \alpha) \dots (h_2 + c - 1 + \alpha)}{(h_1 + a + \alpha) \dots (h_1 + c - 1 + \alpha)}$.

If $h_1 \leq h_2$, then $\text{LHS}_1 \leq \left(\frac{h_1 + a - 1 + \alpha}{h_2 + a - 1 + \alpha}\right)^{a-b}$ and $\text{LHS}_2 \leq \left(\frac{h_2 + c - 1 + \alpha}{h_1 + c - 1 + \alpha}\right)^{a-b}$.

So if $\frac{h_1 + a - 1 + \alpha}{h_2 + a - 1 + \alpha} \leq \frac{n_1 + \beta}{n_2 + \beta}$ then (12) holds, if $\frac{h_2 + c - 1 + \alpha}{h_1 + c - 1 + \alpha} \leq \frac{n_1 + \beta}{n_2 + \beta}$ then (13) holds.

We multiply those two inequalities, and find that $\frac{h_1 + a - 1 + \alpha}{h_2 + a - 1 + \alpha} * \frac{h_2 + c - 1 + \alpha}{h_1 + c - 1 + \alpha} = \frac{h_1 + a - 1 + \alpha}{h_1 + c - 1 + \alpha} * \frac{h_2 + c - 1 + \alpha}{h_2 + a - 1 + \alpha} \leq 1$ as $c > a$ and $h_1 \leq h_2$. But $\frac{n_1 + \beta}{n_2 + \beta} * \frac{n_1 + \beta}{n_2 + \beta} = 1$. At least one equality holds, consequently at least one of (12) and (13) holds.

The proof for case $h_1 > h_2$ follows similarly. □

2.2.3. Randomized K-means. In this section, we illustrate how we estimate parameters for the distribution of weights and demonstrate variability of generated clustering on empirical data. We also investigate the accuracy of random weighting and how it approaches the fully Bayesian scheme in simulation.

To find the value of a_0, a_1 and d_0 , we have the marginal likelihood of $d_{i,j}$

$$P(d_{i,j} | a_0, a_1, d_0) = \frac{\Gamma(a_0 + a_1)}{\Gamma(a_0)\Gamma(a_1)} \frac{d_0^{a_0} d_{i,j}^{a_1 - 1} a_1^{a_1}}{(d_0 + a_1 * d_{i,j})^{a_0 + a_1}}$$

We estimate d_0 by treating $d_{i,j} \approx \Delta_{i,j}$ and based on the mean-variance ratio ($\frac{E(1/\Delta_{i,j})}{\text{Var}(1/\Delta_{i,j})} = d_0$), d_0 can be approximately estimated by moments of $1/d_{i,j}$. Then we obtain a_0, a_1 from MLE of marginal density of $d_{i,j}$. The MLE estimators are obtained through `nlminb` function in R. One issue that arises is that the default value for tolerance rate of stopping is $1e-10$, which yields large value of $a_1 + a_0$ and results in non-randomness of our weighting matrix. To avoid this issue, we set tolerance rate as $1e-3$ to obtain moderate deviation from D (Supplementary Figure S1).

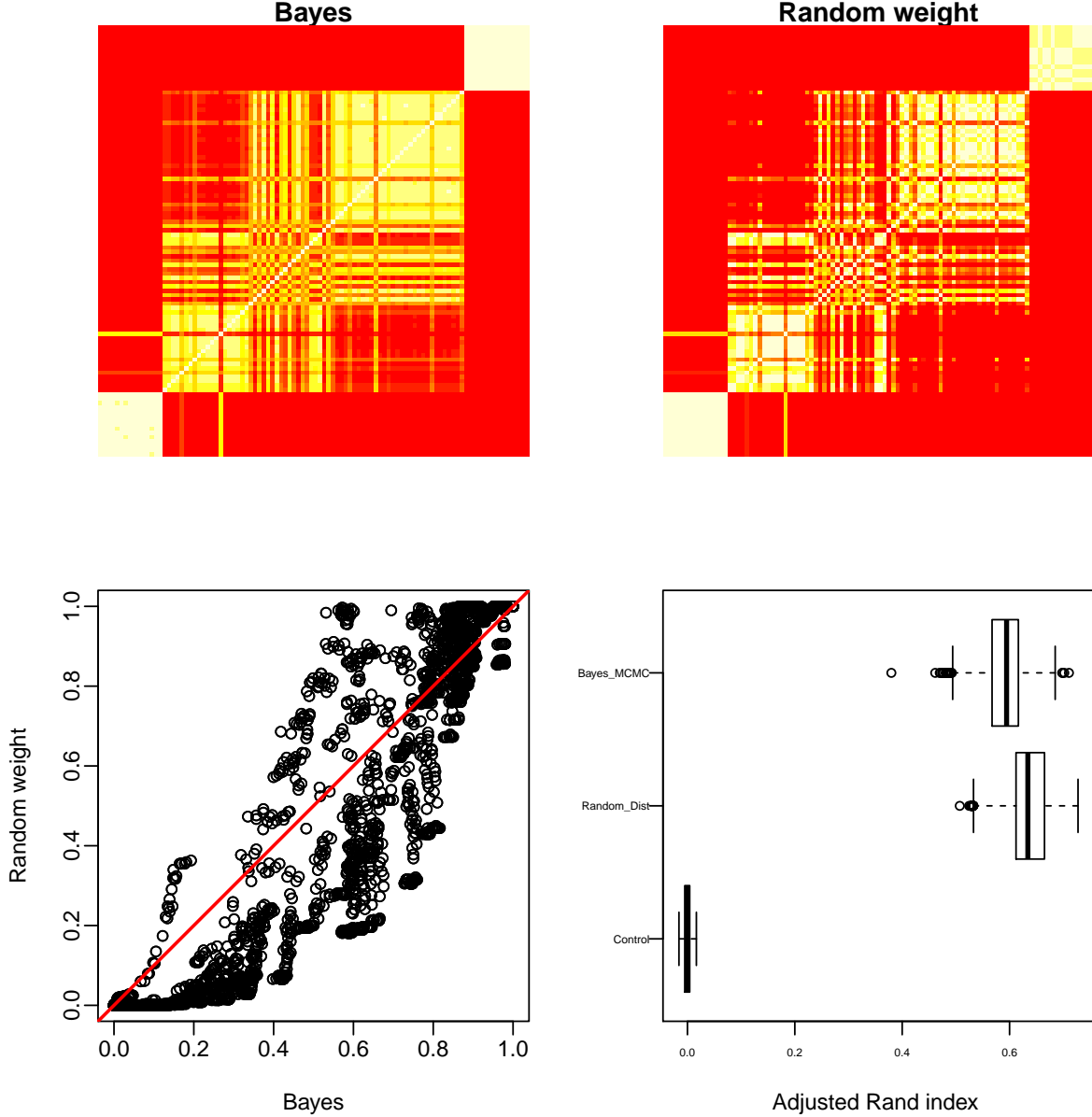


Supplementary Figure S1: Adjusted rand indexes of randomly generated clustering to the one generated by the original distance matrix. We investigate the variation of clustering given by random weighting through 8 datasets and each dataset we are using 100 random distances.

We plot the ARI (adjusted random index) between the randomly generated clustering to clustering under the original distance across eight datasets. Though the mean varies, the interquartile range is wide enough to present a reasonable variation of our random weighting scheme.

We also check validity of random weighting on simulated dataset. We simulate one-dimensional data X from a mixture of 5 normal distributions with different means and same variance ($\mu = (-6, -2, 0, 2, 10), \sigma = 1$). We compare clustering results between random weighting and Bayesian clustering using the Dirichlet process as a prior in terms

of posterior probabilities that two elements belong to the same class given the whole data. We also compare accuracy of the two procedures by looking at the ARI comparing to true class label (Supplementary Figure S2). We found that random weighting scheme tends to give better results than classical Bayesian clustering.



Supplementary Figure S2: Comparison between random weighting scheme and bayesian clustering procedure. Top: heatmap of posterior probabilities that two elements belong to the same class given the whole data. Bottom: scatterplot of these posterior probabilities (left), and adjusted rand index comparing to the underlying true class label (right).

2.2.4. *Selecting K.* In this section, we give the criterion to select K .

To determine the number of clusters, we implement a procedure inspired by validity, as defined in Ray and Turi (2000). We consider a modified validity = $\frac{\text{intra}}{\text{inter}}$, where **intra** =

$\frac{1}{N} \sum_{i=1}^K \sum_{x \in C_i} \|x - z_i\|^2$, **inter** = $\text{mean}(\|z_i - z_j\|^2), i, j = 1, 2, \dots, K$, and z_i is the center (medoid) of cluster i . **intra** is the average of distance of a point to its corresponding cluster center, which measures the compactness of clusters. **inter** is the average distance of two cluster centers, which measures the separation between clusters. In the original paper **inter** was defined as minimum distance between medoids (Ray and Turi, 2000). Here, we instead use the average for the purpose of getting a smoother quantity. We want to have a small intra-cluster distance and a big inter-cluster distance. Consequently we want to minimize validity. From empirical study, we observed that validity is monotonic decreasing with K and this trend stabilizes when K is sufficiently big. The stopping rule for searching K is when $\text{validity}_K < \epsilon$ is satisfied. We set the default value of ϵ to be 1, as we found this yields results most consistent with other scRNA-seq methods.

2.3. Double Dirichlet Mixture. In this section, we give proofs for the properties and theorem for DDM in section 2.3 of main paper.

On the double Dirichlet masses, using notations in the main paper we have density functions:

$$p_\pi(\phi, \psi) = q_\pi(\Phi_\pi, \Psi_\pi) \prod_{b \in \pi} [p(\tilde{\phi}_b) p(\tilde{\psi}_b)]$$

with

$$q_\pi(\Phi_\pi, \Psi_\pi) = \frac{\Gamma(\sum_{b \in \pi} \beta_b)}{\prod_{b \in \pi} \Gamma(\beta_b)} \left[\prod_{b \in \pi} \Phi_b^{\beta_b - 1} \right] 1[\Phi_\pi = \Psi_\pi]$$

and

$$p(\tilde{\phi}_b) = \frac{\Gamma(\sum_{k \in b} \alpha_k)}{\prod_{k \in b} \Gamma(\alpha_k)} \prod_{k \in b} \tilde{\phi}_k^{\alpha_k - 1}, \quad p(\tilde{\psi}_b) = \frac{\Gamma(\sum_{k \in b} \alpha_k)}{\prod_{k \in b} \Gamma(\alpha_k)} \prod_{k \in b} \tilde{\psi}_k^{\alpha_k - 1}.$$

Those computing units will serve as key components for proving property 1 ~ 6 in section 2.3

PROOF OF PROPERTY 1. When ϕ and ψ only satisfy the coarsest constraints: $\sum_{i=1}^K \phi_i = \sum_{i=1}^K \psi_i = 1$. ϕ and ψ are independently Dirichlet distributed. When ϕ and ψ satisfy finer constraints, $P(\phi|\psi) \neq P(\phi)$ as there is some subsets $b \neq \pi$ such that $\sum_{i \in b} \phi = \sum_{i \in b} \psi$. So ϕ and ψ are dependent. \square

PROOF OF PROPERTY 2. $E_\pi(\phi_k) = E_\pi(\phi_k | \Phi_b) E_\Phi(\Phi_b) = E_{\tilde{\phi}_b}(\tilde{\phi}_k) E_\Phi(\Phi_b)$ where b is the block containing subtype index k . As $\tilde{\phi}_b \sim \text{Dirichlet}_{N(b)}[\alpha_b^1]$ and $\Phi_\pi \sim \text{Dirichlet}_{N(\pi)}[\beta_\pi]$ We have $E_{\tilde{\phi}_b}(\tilde{\phi}_k) = \frac{\alpha_k^1}{\sum_{k' \in b} \alpha_{k'}^1}$ and $E_\Phi(\Phi_b) = \frac{\beta_b}{\sum_{b' \in \pi} \beta_{b'}}$. Similarly we could prove the case for $E_\pi(\psi_k)$. \square

PROOF OF PROPERTY 3. t^1/t_π^1 is independent of t^2/t_π^2 conditioning on t_π^1 and t_π^2 by the Neutrality property of Dirichlet distribution \square

PROOF OF PROPERTY 4. For $j = 1, 2$, let T_b^j be the vector of t_k^j such that $k \in b$. Recall $t_b^j = \sum_{k \in b} t_k^j$. Without loss of generality, we consider the case condition $j = 1$. At the support of p_π , for different blocks, $T_b^1|\tilde{\phi}_b$ are mutually independent. Then we have factorization:

$$p_\pi(t^1|t_\pi^1, y) = \prod_{b \in \pi} (p(T_b^1|t_b^1, y))$$

and right hand side prior predictive function can be obtained by integrating out $\tilde{\phi}_b$ given the prior $\text{Dirichlet}[\alpha_b^1]$, and $p(T_b^1|\tilde{\phi}_b)$ is multinomial($\tilde{\phi}_b$) distributed.

$$\begin{aligned} p(T_b^1|t_b^1, y) &= \int_{\tilde{\phi}_b} p(T_b^1|\tilde{\phi}_b) p(\tilde{\phi}_b) d\tilde{\phi}_b \\ &= \left\{ \left[\frac{\Gamma(t_b^1 + 1)}{\prod_{k \in b} \Gamma(t_k^1 + 1)} \right] \left[\frac{\Gamma(\sum_{k \in b} \alpha_k^1)}{\prod_{k \in b} \Gamma(\alpha_k^1)} \right] \left[\frac{\prod_{k \in b} \Gamma(\alpha_k^1 + t_k^1)}{\Gamma(t_b^1 + \sum_{k \in b} \alpha_k^1)} \right] \right\} \end{aligned}$$

\square

PROOF OF PROPERTY 5. t_π^1 and t_π^2 , given the condition label y , are independent and identically distributed. $t_\pi^1|\Phi \sim \text{multinomial}(\Phi)$

$$\begin{aligned} p_\pi(t_\pi^1, t_\pi^2|y) &= \int_{\Phi} p(t_\pi^1|\Phi) p(t_\pi^2|\Phi) p(\Phi) d\Phi \\ &= \left[\frac{\Gamma(n_1 + 1) \Gamma(n_2 + 1)}{\prod_{b \in \pi} \Gamma(t_b^1 + 1) \Gamma(t_b^2 + 1)} \right] \left[\frac{\Gamma(\sum_{b \in \pi} \beta_b)}{\prod_{b \in \pi} \Gamma(\beta_b)} \right] \left[\frac{\prod_{b \in \pi} \Gamma(\beta_b + t_b^1 + t_b^2)}{\Gamma(n_1 + n_2 + \sum_{b \in \pi} \beta_b)} \right]. \end{aligned}$$

As prior of Φ is Dirichlet $[\beta]$ and $n_j = \sum_{b \in \pi} t_b^j$ for $j = 1, 2$. \square

To prove property 6, we need a lemma of dimensionality of the intersection of two A_π s.

LEMMA 1. If π_2 is not refinement of π_1 then $A_{\pi_1} \cap A_{\pi_2}$ is a lower dimensional subset of A_{π_2} .

PROOF OF LEMMA 1. Let V denote the orthogonal space of $\phi - \psi$, when $(\phi, \psi) \in A_{\pi_1} \cap A_{\pi_2}$, and $\dim(A_{\pi_1} \cap A_{\pi_2}) = \dim(\phi - \psi) + \dim(\psi) = 2K - \dim(V) - 1$. Also let $\pi_1 = \{b_1^1, \dots, b_s^1\}$, $\pi_2 = \{b_1^2, \dots, b_t^2\}$. The corresponding vectors are v_1^1, \dots, v_s^1 and v_1^2, \dots, v_t^2 . We claim there must be a $b_i^1 \in \pi$ whose corresponding v_i^1 is linear independent with v_1^2, \dots, v_t^2 . If not, for every v_i^1 there exists $\alpha_1^i, \dots, \alpha_t^i$ such that

$$v_i^1 = \sum_{j=1}^t \alpha_j^i v_j^2 \quad (*)$$

If $b_j^2 \cap b_i^1 \neq \emptyset$, then multiply v_j^2 on both sides of (*), we obtain $v_i^1 * v_j^2 = \alpha_j^i (v_j^2)^2$, as v_j^2 are orthogonal vectors, and $v_i^1 * v_j^2 > 0$ implies $\alpha_j^i > 0$. Consider $x = f(b_j^2 \setminus b_i^1)$. We have $x * v_i^1 = 0$ and multiply x on both sides of (*) to obtain $\alpha_j^i v_j^2 * x = 0$. Thus x must be zero vector and $b_j^2 \setminus b_i^1 = \emptyset$, which implies $b_j^2 \subset b_i^1$. That is to say when $b_j^2 \cap b_i^1 \neq \emptyset$, b_j^2 must be subset of b_i^1 . So b_i^1 is union of some blocks in π_2 . This implies π_2 is refinement of π_1 : a contradiction.

Consequently, there exists $b \in \pi_1$ with $v(b)$ linear independent with $v(b'), b' \in \pi_2$. $\dim(V)$ is at least $N(\pi_2) + 1, \dim(A_{\pi_1} \cap A_{\pi_2}) < \dim(A_{\pi_2})$. \square

PROOF OF PROPERTY 6. For a π , $P(A_\pi, |y, z) = \sum_{\tilde{\pi} \in \Pi} \int_{A_\pi} \omega_{\tilde{\pi}}^{\text{post}} d\phi d\psi$, notice the support of $\omega_{\tilde{\pi}}^{\text{post}}$ is $A_{\tilde{\pi}}$. By lemma 1, we know if $\tilde{\pi}$ does not refine π , then $\int_{A_\pi} \omega_{\tilde{\pi}}^{\text{post}} d\phi d\psi$ is an integral on lower dimension set and vanishes. if $\tilde{\pi}$ refines π , then $\int_{A_\pi} \omega_{\tilde{\pi}}^{\text{post}} d\phi d\psi = \int_{A_{\tilde{\pi}}} \omega_{\tilde{\pi}}^{\text{post}} d\phi d\psi = \omega_{\tilde{\pi}}^{\text{post}}$. We have $P(A_\pi, |y, z) = \sum_{\tilde{\pi} \in \Pi} \omega_{\tilde{\pi}}^{\text{post}} 1[\tilde{\pi} \text{ refines } \pi]$. \square

PROOF OF THEOREM 3. Recall the DDM prior: $p(\phi, \psi) = \sum_{\pi \in \Pi} p_\pi(\phi, \psi)$. By bayes' rule we know $p(\phi, \psi | y, z) \propto p(\phi, \psi, y, z) = \sum_{\pi \in \Pi} p(y, z | \phi, \psi) p_\pi(\phi, \psi) \omega_\pi$ and we use the 1-1 map from (ϕ, ψ) to $(\tilde{\phi}, \tilde{\psi}, \Phi)$ to get

$$p(y, z | \phi, \psi) p_\pi(\phi, \psi) = p(y, z | \tilde{\phi}, \tilde{\psi}, \Phi_\pi) p(\tilde{\phi}) p(\tilde{\psi}) p(\Phi_\pi)$$

when $(\phi, \psi) \in A_\pi$. Let us denote right hand side of the above equation as U_π , then

$$U_\pi = \omega_\pi A_1 A_2 A_3 \prod_{k=1}^K (\tilde{\phi}_k)^{t_k^1 + \alpha_k^1} (\tilde{\psi}_k)^{t_k^2 + \alpha_k^2} \prod_{b \in \pi} (\Phi_b)^{t_b^1 + t_b^2 + \beta_b}$$

Where A_1 is the product of normalizing terms from multinomial distribution of z^1 and z^2 , $A_1 = \frac{\Gamma(n_1+1)\Gamma(n_2+1)}{\prod_{j=1}^2 \prod_{k=1}^K \Gamma(t_k^j+1)}$.

A_2 is the product of normalizing terms from Dirichlet distribution of $\tilde{\phi}$ and $\tilde{\psi}$, $A_2 = \frac{\Gamma(\sum_{k=1}^K \alpha_k^1 + 1) \Gamma(\sum_{k=1}^K \alpha_k^2 + 1)}{\prod_{j=1}^2 \prod_{k=1}^K \Gamma(\alpha_k^j + 1)}$.

A_3 is the normalizing term from Dirichle distribution of Φ_π , $A_3 = \frac{\Gamma(\sum_{b \in \pi} \beta_b + 1)}{\prod_{b \in \pi} \Gamma(\beta_b + 1)}$.

Looking at the indexes of $\tilde{\phi}, \tilde{\psi}$ and Φ , we can decompose U_π as a product of three Dirichlet densities with a normalizing term. Namely $U_\pi = C_\pi * f_1 f_2 f_3$, where $f_1 \sim \text{Dirichlet}[\alpha^1 + t^1]$, $f_2 \sim \text{Dirichlet}[\alpha^2 + t^2]$ and $f_3 \sim \text{Dirichlet}[\beta + t^1 + t^2]$. Considering the normalizing factors for densities f_1, f_2 and f_3 , and multiplying them with A_1, A_2 and A_3 , we have $C_\pi = p_\pi(t^1 | t_\pi^1, y) p_\pi(t^2 | t_\pi^2, y) p_\pi(t_\pi^1, t_\pi^2 | y) \omega_\pi$.

Consequently, we have

$$(\phi, \psi) | y, z \sim \text{DDM} \left[\omega^{\text{post}} = (\omega_\pi^{\text{post}}), \alpha^1 + t^1, \alpha^2 + t^2 \right] \text{ and } \omega_\pi^{\text{post}} \propto p_\pi(t^1 | t_\pi^1, y) p_\pi(t^2 | t_\pi^2, y) p_\pi(t_\pi^1, t_\pi^2 | y) \omega_\pi$$

Notice in DDM, we restricted $\beta = \alpha^1 + \alpha^2$. \square

3. Numerical Experiments.

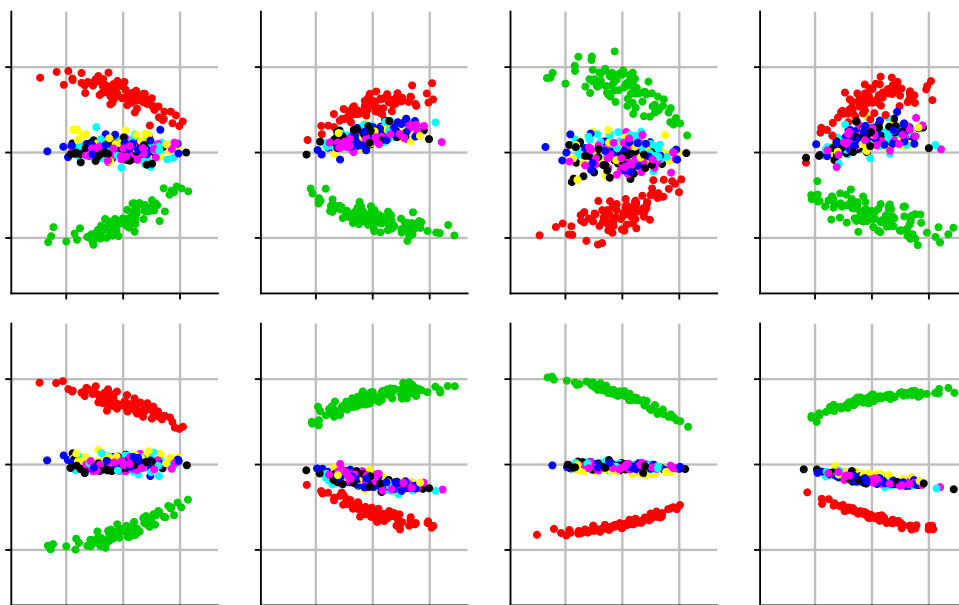
3.1. *Synthetic Data.* In this section, we use PCA plots to show the subtle changes underlying each subtype of simulated data and we demonstrate consistency of estimated distributional changes based on scDDboost and Wasserstein distance. Finally, ROC curves illustrate that scDDboost has favorable operating characteristics.

We first look at the PCA plots of the simulated data (Supplementary Figure S3, S4, S5). For $K = 7$ and 12, in each scenario there were some subtypes nested in the 2d PCA projection and the distributional change of transcripts becomes difficult to detect. scDDboost benefits from the compositional structure and is more sensitive to those subtle changes.

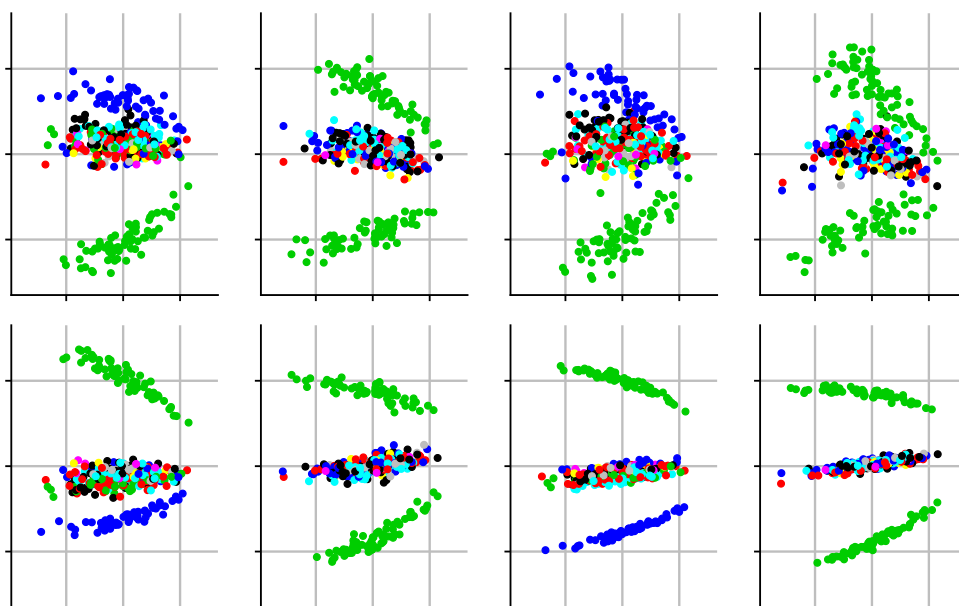


Supplementary Figure S3: first two principal components of transcripts under different parameters for simulated data. Horizontal axis refers to first component, vertical axis refers to second component. Different parameters resulted in different degree of separation of subtypes. We have 4 different settings for hyper-parameters of simulation, each setting has 2 replicates. From left to right, the associated hyper-parameters are $(0.1, 0.4)$, $(-0.1, 0.3)$, $(0.3, 0.5)$, $(-0.1, 1)$. Here we have 3 subtypes

We observed consistent measurements of distributional change by scDDboost and Wasserstein distance (Supplementary Figure S6). Lower probabilities of equivalent distributed are associated with bigger distances.



Supplementary Figure S4: similar plots as Supplementary Figure S3, but for 7 subtypes



Supplementary Figure S5: similar plots as Supplementary Figure S3, but for 12 subtypes



Supplementary Figure S6: $P(ED_g | X, y)$ given by scDDboost versus empirical Wasserstein distance. Genes associated with boxes from left to right having $P(ED_g | X, y)$ range from 0 - 0.2, 0.2 - 0.4, 0.4 - 0.6, 0.6 - 0.8, 0.8 - 1. For simulation cases with parameters in the format: number of clusters / shape / scale

We also show ROC curves for the simulated data in Supplementary Figure S7. here each sub-figure is averaged over two replicates under the same parameters setting. scD-Dboost tends to outperform other methods .



Supplementary Figure S7: Roc curve of the 12 simulation settings, under each setting, TPR and FPR are averaged over two replicates, generally we found scDDboost perform better than other methods

3.2. *Empirical Study.* In this section, we provide details of the empirical datasets and also demonstrate consistency to Wasserstein distance on one dataset FUCCI (Leng et al., 2015).

Data sets Details for the datasets used in the empirical studies of the main paper and the estimated number of subtypes K are shown in Supplementary Table S1.

| Data set | Conditions | Number of cells/condition | Organism | Ref | K |
|-------------------|--|---------------------------|----------|-------------------------|---|
| GSE94383 | 0 min unstim vs 75min stim | 186,145 | human | (Lane et al., 2017) | 9 |
| GSE48968-GPL13112 | BMDC (2h LPS stimulation) vs 6h LPS | 96,96 | mouse | (Shalek et al., 2014) | 4 |
| GSE52529 | T0 vs T72 | 69,74 | human | (Trapnell et al., 2014) | 7 |
| GSE74596 | NKT1 vs NTK2 | 46,68 | mouse | (Engel et al., 2016) | 7 |
| EMTAB2805 | G1 vs G2M | 95,96 | mouse | (Buettner et al., 2015) | 6 |
| GSE71585-GPL13112 | Gad2tdTpositive vs Cux2tdTnegative | 80,140 | mouse | (Tasic et al., 2016) | 4 |
| GSE64016 | G1 vs G2 | 91,76 | human | (Leng et al., 2015) | 6 |
| GSE79102 | patient1 vs patient2 | 51, 89 | human | Kiselev et al. (2017) | 4 |
| GSE45719 | 16-cell stage blastomere vs mid blastocyst cell | 50, 60 | mouse | (Deng et al., 2014) | 4 |
| GSE63818 | Primordial Germ Cells, developmental stage: 7 week gestation vs Somatic Cells, developmental stage: 7 week gestation | 40,26 | mouse | (Guo et al., 2015) | 6 |
| GSE75748 | DEC vs EC | 64, 64 | human | (Chu et al., 2016) | 5 |
| GSE84465 | neoplastic cells vs non-neoplastic cells | 1000, 1000 | human | (Darmanis et al., 2017) | 9 |

SUPPLEMENTARY TABLE S1
datasets used for comparisons of DD analysis under different methods

For the first 11 datasets in supplementary table S1 we use all the cells within that condition under same batch. The last one is the largest dataset we explored containing 3589 cells and comparing neoplastic cells (1091 cells) vs non-neoplastic cells (2498 cells). We randomly sampled 1000 cells from each condition, because it takes a lot of time for DESeq and scDD to compute when using all the samples and we conjecture that 1000 cells each condition would be enough to represent the heterogeneity. We run the comparison on those subsamples instead and found DESeq identified significantly smaller numbers of positives than other methods. It is intuitive that we are more likely to encounter subtle changes when we have large samples, and only considering mean shifts would have limited power.

We also observed consistent distributional change measurements by scDDboost and Wasserstein distance (Supplementary Figure S8).



Supplementary Figure S8: $P(ED_g|X, y)$ given by scDDboost versus empirical Wasserstein distance. Genes associated with boxes from left to right having $P(ED_g|X, y)$ range from 0 - 0.2, 0.2 - 0.4, 0.4 - 0.6, 0.6 - 0.8, 0.8 - 1, data used: FUCCI

Datasets used for generating the Null cases are shown in Supplementary Table S2.

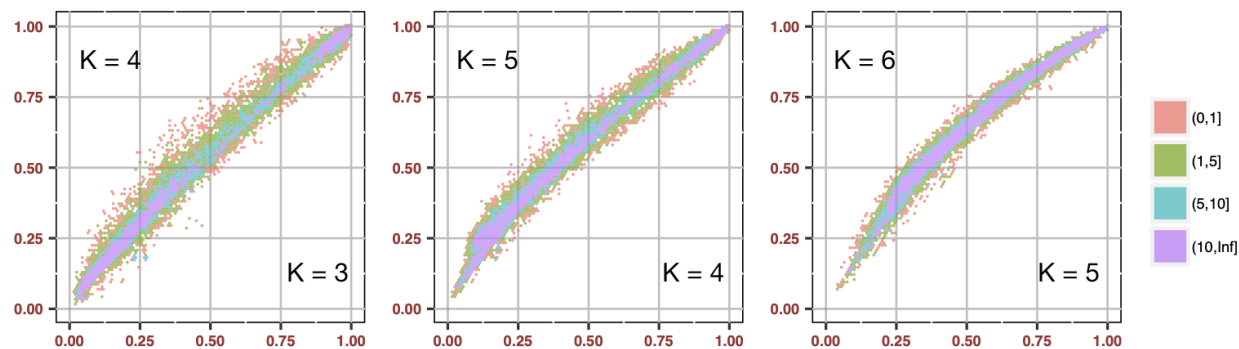
| Data set | Conditions | Number of cells/condition | Organism |
|-----------------------|---------------------------|---------------------------|----------|
| GSE63818null | 7 week gestation | 20,20 | mouse |
| GSE75748null | DEC | 32, 32 | human |
| GSE94383null | T0 | 93, 93 | human |
| GSE48968-GPL13112null | BMDC (2h LPS stimulation) | 48,48 | mouse |
| GSE74596null | NKT1 | 23,23 | mouse |
| EMTAB2805null | G1 | 48,48 | mouse |
| GSE71585-GPL13112null | Gad2tdTpositive | 40,40 | mouse |
| GSE64016null | G1 | 46,45 | human |
| GSE79102null | patient1 | 26, 25 | human |

SUPPLEMENTARY TABLE S2
datasets used for null cases, as cells are coming from same biological condition, there should not be any differential distributed genes, any positive call is false positive

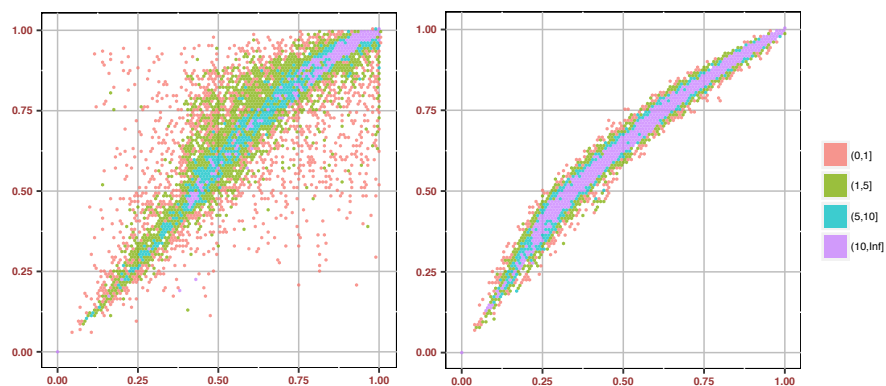
3.3. *Robustness.* In this section, we demonstrate change of PDD under different K and the robustness we gain through random weighting. We also give a warning that using arbitrarily large K will inflate FDR.

the number of subtypes K is a crucial parameter controlling the accuracy of our modeling. Too small K may end up underfitting such that cells within same subtype can still be very different, the mean expression change among subtypes is incapable to capture the marginal distribution change. Consequently reducing the power of scDDboost. Too big K may end up overfitting such that two subtypes can be very similar. Given that we have a fixed number of cells, allowing more clusters will not only increase the burden of computation but decrease the certainty of our inference on DE pattern.

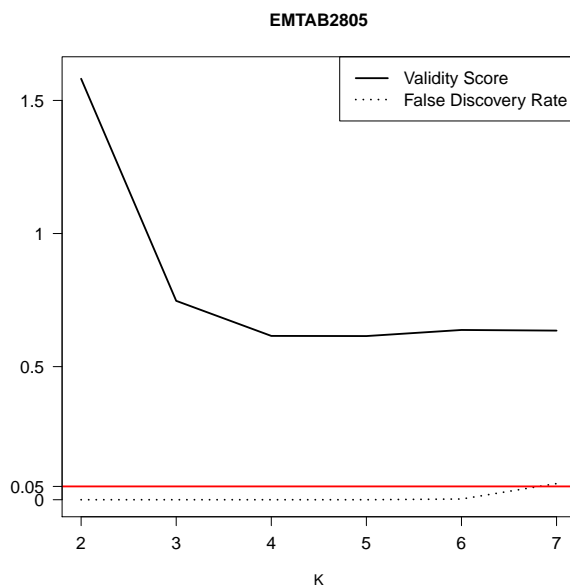
From our empirical experience, it is sufficient to capture the heterogeneity underlying cells with number of clusters less than 10 (K in Supplementary TableS1). To demonstrate the change of PDD given different K , we present an example using dataset GSE75748. When we increase K , the variance of the differential term $PDD_{K+1} - PDD_K$ keeps decreasing and PDD keeps increasing. Our selection criterion ($K = 5$) happens to choose K such that change between PDD_{K+1} and PDD_K is small while not inflating PDD. We generally obtain stable validity score and PDD simultaneously (Supplementary Figure S9). In addition, the random weighting scheme help us obtain robust PDD (Supplementary Figure S10). There is one thing we need to be cautious, scDDboost may lose FDR control if we keep increasing K (Supplementary Figure S11). But from our simulation study, our selecting rule never overestimate K .



Supplementary Figure S9: PDD change under different number of subtypes K for dataset DEC-EC (GSE75748). Our rule for selecting K tends also to make PDD stabilize.



Supplementary Figure S10: PDD under $K = 5$ vs. $K = 6$ for dataset DEC-EC (GSE75748). Left panel is without the randomized distance and right panel is with randomized distance. We increase robustness of our methods through random weighting.



Supplementary Figure S11: under NULL case, using dataset EMTAB2805, when using too big K we may lose FDR control (black dashed line shows proportion of false positive identified by scDDboost under 0.05 threshold, while validity score did not vary too much after K is greater than 2).

4. Posterior consistency. In this section, we prove theorem 4.

The density of DDM is computed by product or ratio over several gamma functions and the gamma function is not easy to directly derive limiting theorem. To prove theorem 4, we need a crucial lemma which gives us an approximation to the gamma function, namely

LEMMA 2. For $x \geq 1$, $\frac{x^{x-c}}{e^{x-1}} \leq \Gamma(x) \leq \frac{x^{x-1/2}}{e^{x-1}}$, where $c = 0.577215\dots$ is the Euler-Mascheroni constant.

PROOF. By (Li and ping Chen, 2007), we have $\frac{x^{x-c}}{e^{x-1}} \leq \Gamma(x) \leq \frac{x^{x-1/2}}{e^{x-1}}$ for $x > 1$ and now we added the case when $x = 1, \Gamma(x) = 1$ so that both sides will include the equality case. \square

We have another lemma and theorem 4 is just proposition of the lemma

LEMMA 3. If $(\phi, \psi) \in A_{\pi_1} \cap A_{\pi_2}$, follow the conditions in theorem 1 then

$$\frac{\omega_{\pi_1}^{post}}{\omega_{\pi_2}^{post}} \xrightarrow[n \rightarrow \infty]{a.s.} 0 \quad \text{if } N(\pi_1) < N(\pi_2)$$

PROOF. Recall $\omega_{\pi}^{post} \propto p_{\pi}(t^1 | t_{\pi}^1, y) p_{\pi}(t^2 | t_{\pi}^2, y) p_{\pi}(t_{\pi}^1, t_{\pi}^2 | y) \omega_{\pi}$ and
 RHS = $g(\pi, \alpha, \beta, n_1, n_2) f(\pi, t^1, t^2, \alpha, \beta)$ and $\frac{\omega_{\pi_1}^{post}}{\omega_{\pi_2}^{post}} = \frac{g(\pi_1, \alpha, \beta, n_1, n_2)}{g(\pi_2, \alpha, \beta, n_1, n_2)} \frac{f(\pi_1, t^1, t^2, \alpha, \beta)}{f(\pi_2, t^1, t^2, \alpha, \beta)}$ where

$$g(\pi, t^1, t^2, \alpha, \beta) = \left[\prod_{j=1}^2 \prod_{b \in \pi} \prod_{k \in b} \frac{\Gamma(\sum_{k \in b} \alpha_k^j)}{\Gamma(\alpha_k^j)} \right] \frac{\Gamma(n_1 + 1) \Gamma(n_2 + 1)}{\prod_{b \in \pi} \Gamma(\beta_b)} \frac{\Gamma(\sum_{b \in \pi} \beta_b)}{\Gamma(n_1 + n_2 + \sum_{b \in \pi} \beta_b)}$$

$$f(\pi, t^1, t^2, \alpha, \beta) = \left[\prod_{j=1}^2 \prod_{b \in \pi} \prod_{k \in b} \frac{1}{\Gamma(t_k^j + 1)} \frac{\prod_{k \in b} \Gamma(\alpha_k^j + t_k^j)}{\Gamma(t_b^j + \sum_{k \in b} \alpha_k^j)} \right] \prod_{b \in \pi} \Gamma(\beta_b + t_b^1 + t_b^2)$$

For notation simplicity, we use the abbreviation $g(\pi), f(\pi)$ to substitute

$g(\pi, \alpha, \beta, n_1, n_2), f(\pi, t^1, t^2, \alpha, \beta)$. We take log on $\frac{\omega_{\pi_1}^{post}}{\omega_{\pi_2}^{post}}$, denote it as LR. $LR = \ln g(\pi_1) - \ln g(\pi_2) + \ln f(\pi_1) - \ln f(\pi_2)$. Denote $C(\pi_1, \pi_2, \alpha, \beta) = \ln g(\pi_1) - \ln g(\pi_2)$, $C(\pi_1, \pi_2, \alpha, \beta)$ does not change with sample size n_1, n_2 and is a constant determined by partition π_1, π_2 and hyper parameters α, β . For further convenience of notation let $h(x) = \ln \Gamma(x)$ and $\gamma_b^j = \sum_{k \in b} \alpha_k^j$. Denote $R(\pi_1, \pi_2, t^1, t^2, \alpha, \beta) = \ln f(\pi_1) - \ln f(\pi_2)$. And removing the common part of $f(\pi_1)$ and $f(\pi_2)$, we have

$$R(\pi_1, \pi_2, t^1, t^2, \alpha, \beta) = d(\pi_1, t^1, t^2, \alpha, \beta) - d(\pi_2, t^1, t^2, \alpha, \beta)$$

where

$$d(\pi, t^1, t^2, \alpha, \beta) = \sum_{b \in \pi} h(\beta_b + t_b^1 + t_b^2) - \sum_{j=1}^2 \sum_{b \in \pi} h(t_b + \gamma_b^j)$$

Recall $\beta_b = \gamma_b^1 + \gamma_b^2$ and from lemma 2, $(x - c)\ln(x) - x + 1 \leq h(x) \leq (x - 1/2)\ln(x) - x + 1$ we have

(3)

$$d(\pi, t^1, t^2, \alpha, \beta) \geq \sum_{b \in \pi} (\beta_b + t_b^1 + t_b^2 - c) \ln(\beta_b + t_b^1 + t_b^2) - \sum_{j=1}^2 \sum_{b \in \pi} (t_b^j + \gamma_b^j - 1/2) \ln(t_b^j + \gamma_b^j) + N(\pi)$$

(4)

$$d(\pi, t^1, t^2, \alpha, \beta) \leq \sum_{b \in \pi} (\beta_b + t_b^1 + t_b^2 - 1/2) \ln(\beta_b + t_b^1 + t_b^2) - \sum_{j=1}^2 \sum_{b \in \pi} (t_b^j + \gamma_b^j - c) \ln(t_b^j + \gamma_b^j) + N(\pi)$$

$$\begin{aligned} \text{RHS of (4)} &= \sum_b [(t_b^1 + \gamma_b^1) \ln(1 + \frac{t_b^2 + \gamma_b^2}{t_b^1 + \gamma_b^1}) + (t_b^2 + \gamma_b^2) \ln(1 + \frac{t_b^1 + \gamma_b^1}{t_b^2 + \gamma_b^2}) \\ &\quad + (1 - c) \ln(\beta_b + t_b^1 + t_b^2) - 1/2 (\ln(1 + \frac{t_b^2 + \gamma_b^2}{t_b^1 + \gamma_b^1}) + \ln(1 + \frac{t_b^1 + \gamma_b^1}{t_b^2 + \gamma_b^2}))] + N(\pi) \end{aligned}$$

By Taylor expansion at $x = 1$, $\ln(x + 1) = \ln 2 + 1/2(x - 1) - 1/8(x - 1)^2 + g(\xi)(x - 1)^3$, where $g(\xi)$ is the reminder term of form $\frac{1}{3(1+\xi)^3}$ for $0 < \xi < x$ For a fixed n_1, n_2 , we have

$$\begin{aligned} \text{RHS of (4)} &= (n_1 + n_2) \ln 2 - \sum_{b \in \pi} (1/8(X_b^1 + X_b^2) \\ &\quad + g(\xi_b)(Y_b^1 + Y_b^2)) + T(\pi) + N(\pi) \end{aligned}$$

$$\text{where } X_b^1 = \frac{(t_b^1 - t_b^2 + \gamma_b^1 - \gamma_b^2)^2}{t_b^1 + \gamma_b^1}, X_b^2 = \frac{(t_b^1 - t_b^2 + \gamma_b^1 - \gamma_b^2)^2}{t_b^2 + \gamma_b^2}, Y_b^1 = \frac{(t_b^1 - t_b^2 + \gamma_b^1 - \gamma_b^2)^3}{(t_b^1 + \gamma_b^1)^2}, Y_b^2 = \frac{(t_b^1 - t_b^2 + \gamma_b^1 - \gamma_b^2)^3}{(t_b^2 + \gamma_b^2)^2}$$

$$\text{and } T(\pi) = \sum_{b \in \pi} [(1 - c) \ln(\beta_b + t_b^1 + t_b^2) - 1/2 (\ln(1 + \frac{t_b^2 + \gamma_b^2}{t_b^1 + \gamma_b^1}) + \ln(1 + \frac{t_b^1 + \gamma_b^1}{t_b^2 + \gamma_b^2}))]$$

Similarly

$$\begin{aligned} \text{RHS of (5)} &= (n_1 + n_2) \ln 2 - \sum_{b \in \pi} (1/8(X_b^1 + X_b^2) \\ &\quad + g(\xi_b)(Y_b^1 + Y_b^2)) + U(\pi) + N(\pi) \end{aligned}$$

$$U(\pi) = \sum_{b \in \pi} [(2c - 1/2) \ln(\beta_b + t_b^1 + t_b^2) - c (\ln(1 + \frac{t_b^2 + \gamma_b^2}{t_b^1 + \gamma_b^1}) + \ln(1 + \frac{t_b^1 + \gamma_b^1}{t_b^2 + \gamma_b^2}))]$$

Using above inequalities, we have

$$\begin{aligned} R(\pi_1, \pi_2, t^1, t^2, \alpha, \beta) &\leq U(\pi_1) - T(\pi_2) - 1/8 (\sum_{b \in \pi_1} (X_b^1 + X_b^2) - \sum_{b \in \pi_2} (X_b^1 + X_b^2)) \\ &\quad + \sum_{b \in \pi_1} g(\xi_b)(Y_b^1 + Y_b^2) - \sum_{b \in \pi_2} g(\xi_b)(Y_b^1 + Y_b^2) \end{aligned}$$

$Y_b^j = \frac{((t_b^1 - t_b^2 + \gamma_b^1 - \gamma_b^2)/\sqrt{n})^3/\sqrt{n}}{((t_b^j + \gamma_b^j)/n)^2}$, by LLN the denominator goes to a constant and by CLT in the numerator $(t_b^1 - t_b^2 + \gamma_b^1 - \gamma_b^2)/\sqrt{n} \rightarrow (t_b^1 - t_b^2)/\sqrt{n} \rightarrow \sqrt{n}[(t_b^1/n - \Phi_b) - (t_b^2/n -$

$\Psi_b]$, which goes to a normal distributed random variable when $\Phi_b = \Psi_b$. So Y_b^j is $o_p(1)$. Similarly, $X_b^j = \frac{((t_b^1 - t_b^2 + \gamma_b^1 - \gamma_b^2)/\sqrt{n})^2}{t_b^j + \gamma_b^j/n}$ is asymptotic gamma (χ -square) distributed. $g(\xi_b)$ has bounded variance, $U(\pi_1) - T(\pi_2) = -\ln(n)$ if $N(\pi_2) < N(\pi_1)$ as $\ln(\beta_b + t_b^1 + t_b^2) - \ln(\beta_{b'} + t_{b'}^1 + t_{b'}^2) = \ln(\frac{\beta_b + t_b^1 + t_b^2}{n}) - \ln(\frac{\beta_{b'} + t_{b'}^1 + t_{b'}^2}{n}) \rightarrow O(1)$ a.s. so we complete the proof. \square

Proof of theorem 4

PROOF. Recall $\sum_{\pi \in \Pi} \omega_\pi^{\text{post}} = 1$ and $P(A_\pi | y, z) = \sum_{\tilde{\pi} \in \Pi} \omega_{\tilde{\pi}}^{\text{post}} 1[\tilde{\pi} \text{ refines } \pi]$. If $(\phi, \psi) \notin Q$, for all the A_π covers (ϕ, ψ) there is one finest π^* with the largest $N(\pi^*)$ and every other π that $(\phi, \psi) \in A_\pi$ is coarser than π^* . We get the results of theorem 4 by lemma 4. \square

References.

- BUETTNER, F., NATARAJAN, K. N., CASALE, F. P., PROSERPIO, V., SCIALDONE, A., THEIS, F. J., TEICHMANN, S. A., MARI-
ONI, J. C. and STEGLE, O. (2015). Computational analysis of cell-to-cell heterogeneity in single-cell RNA-sequencing
data reveals hidden subpopulations of cells. *Nature Biotechnology* **33** 155 EP -.
- CHU, L.-F., LENG, N., ZHANG, J., HOU, Z., MAMOTT, D., VEREIDE, D. T., CHOI, J., KENDZIORSKI, C., STEWART, R. and
THOMSON, J. A. (2016). Single-cell RNA-seq reveals novel regulators of human embryonic stem cell differentiation
to definitive endoderm. *Genome Biology* **17** 173. .
- DAHL, D. B. (2009). Modal clustering in a class of product partition models. *Bayesian Anal.* **4** 243–264.
- DARMANIS, S., SLOAN, S. A., CROOTE, D., MIGNARDI, M., CHERNIKOVA, S., SAMGHABABI, P., ZHANG, Y., NEFF, N.,
KOWARSKY, M., CANEDA, C., LI, G., CHANG, S. D., CONNOLLY, I. D., LI, Y., BARRES, B. A., GEPHART, M. H. and
QUAKE, S. R. (2017). Single-Cell RNA-Seq Analysis of Infiltrating Neoplastic Cells at the Migrating Front of Human
Glioblastoma. *Cell reports* **21** 1399–1410.
- DENG, Q., RAMSKÖLD, D., REINIUS, B. and SANDBERG, R. (2014). Single-Cell RNA-Seq Reveals Dynamic, Random
Monoallelic Gene Expression in Mammalian Cells. *Science* **343** 193–196.
- ENGEL, I., SEUMOIS, G., CHAVEZ, L., SAMANIEGO-CASTRUITA, D., WHITE, B., CHAWLA, A., MOCK, D., VIJAYANAND, P.
and KRONENBERG, M. (2016). Innate-like functions of natural killer T cell subsets result from highly divergent gene
programs. *Nature Immunology* **17** 728 EP -.
- GUO, F., YAN, L., GUO, H., LI, L., HU, B., ZHAO, Y., YONG, J., HU, Y., WANG, X., WEI, Y., WANG, W., LI, R., YAN, J., ZHI, X.,
ZHANG, Y., JIN, H., ZHANG, W., HOU, Y., ZHU, P., LI, J., ZHANG, L., LIU, S., REN, Y., ZHU, X., WEN, L., GAO, Y. Q.,
TANG, F. and QIAO, J. (2015). The Transcriptome and DNA Methylation Landscapes of Human Primordial Germ
Cells. *Cell* **161** 1437–1452.
- KISELEV, V. Y., KIRSCHNER, K., SCHAUB, M. T., ANDREWS, T., YIU, A., CHANDRA, T., NATARAJAN, K. N., REIK, W.,
BARAHONA, M., GREEN, A. R. and HEMBERG, M. (2017). SC3: consensus clustering of single-cell RNA-seq data.
Nature Methods **14** 483 EP -.
- LANE, K., VAN VALEN, D., DEFELICE, M. M., MACKLIN, D. N., KUDO, T., JAIMOVICH, A., CARR, A., MEYER, T., PE’ER, D.,
BOUTET, S. C. and COVERT, M. W. (2017). Measuring Signaling and RNA-Seq in the Same Cell Links Gene Expression
to Dynamic Patterns of NF- κ B Activation. *Cell Systems* **4** 458–469.e5.
- LENG, N., CHU, L.-F., BARRY, C., LI, Y., CHOI, J., LI, X., JIANG, P., STEWART, R. M., THOMSON, J. A. and KENDZIORSKI, C.
(2015). Oscop identifies oscillatory genes in unsynchronized single-cell RNA-seq experiments. *Nature Methods* **12**
947 EP -.
- LI, X. and PING CHEN, C. (2007). Inequalities for the gamma function. In 2007), Art. 28. [ONLINE: <http://ijipam.vu.edu.au/article.php?sid=842>].
- RAY, S. and TURI, R. H. (2000). Determination of Number of Clusters in K-Means Clustering and Application in Colour
Image Segmentation.
- SHALEK, A. K., SATIJA, R., SHUGA, J., TROMBETTA, J. J., GENNERT, D., LU, D., CHEN, P., GERTNER, R. S., GAUBLomme, J. T.,
YOSEF, N., SCHWARTZ, S., FOWLER, B., WEAVER, S., WANG, J., WANG, X., DING, R., RAYCHOWDHURY, R., FRIEDMAN, N.,

- HACOHEN, N., PARK, H., MAY, A. P. and REGEV, A. (2014). Single-cell RNA-seq reveals dynamic paracrine control of cellular variation. *Nature* **510** 363 EP -.
- TASIC, B., MENON, V., NGUYEN, T. N., KIM, T. K., JARSKY, T., YAO, Z., LEVI, B., GRAY, L. T., SORENSEN, S. A., DOLBEARE, T., BERTAGNOLLI, D., GOLDY, J., SHAPOVALOVA, N., PARRY, S., LEE, C., SMITH, K., BERNARD, A., MADISEN, L., SUNKIN, S. M., HAWRYLYCZ, M., KOCH, C. and ZENG, H. (2016). Adult mouse cortical cell taxonomy revealed by single cell transcriptomics. *Nature Neuroscience* **19** 335 EP -.
- TRAPNELL, C., CACCHIARELLI, D., GRIMSBY, J., POKHAREL, P., LI, S., MORSE, M., LENNON, N. J., LIVAK, K. J., MIKKELSEN, T. S. and RINN, J. L. (2014). The dynamics and regulators of cell fate decisions are revealed by pseudotemporal ordering of single cells. *Nature biotechnology* **32** 381–386.